Large-disturbance Stability Analysis of Power Systems with Synchronous Generator and Converter-interfaced Generation

Lei Chen, *Senior Member*, *IEEE*, Yong Min, *Member*, *IEEE*, Liangshuai Hao, Guangzheng Xing, *Student Member*, *IEEE*, Yalou Li, and Shiyun Xu

***Abstract*—This letter studies large-disturbance stability of the power system with a synchronous generator (SG) and a converter-interfaced generation (CIG) connected to infinite bus. The power system is multi-timescale and first simplified. It is shown that the boundary of region of attraction (ROA) of the simplified model is composed of stable manifolds of unstable equilibrium point (UEP) or semi-singular point (SSP), named anchor points, and singular surface pieces. The type of anchor point determines the dominant instability pattern of the power system. When the anchor point is UEP or SSP, the dominant instability pattern is the instability of rotor angle of SG or the instability of phase-locked loop and outer control loop (OCL) of CIG, respectively. Transition of dominant instability pattern can be analyzed with the relative position relationship between UEP and SSP. The effect of OCL is discussed. When the OCL is activated, the ROA becomes smaller and the system is more prone to instability of CIG. It is necessary to consider the OCL when studying the large-disturbance stability of the power system.**

***Index Terms*—Converter-interfaced generation, large-disturbance stability, outer control loop, phase-locked loop, synchronous generator, voltage source converter.**

I. Introduction

LARGE-DISTURBANCE stability is an important category of power system stability. Large-disturbance rotor angle stability or transient stability of synchronous generators (SGs) has been studied thoroughly. More and more converter-interfaced generations (CIGs) are connected to the power system, which greatly affect the stability. Large-disturbance stability of CIG connected to infinite bus, mainly synchronization stability, has been studied a lot, but few research focuses on the stability of a mixed system containing both SG and CIG [1], [2], which is a widely existing system form yet.

In the mixed system, the classic transient stability of SG is certainly affected by CIG. The impact of CIG on the power system transient stability is analytically investigated in [2]. It is found that CIG changes the original power-angle relationship of SG into a non-sinusoidal curve, and introduces a limit on the peak of the rotor swing. The maximum of the SG's rotor angle movement is limited by the synchronization of phase-locked loop (PLL). However, the outer control loop (OCL) is ignored in [2].

During a short-circuit fault, a CIG often switches to current-controlled mode and the OCL is deactivated, but when the fault is cleared, the OCL is activated again. Large-disturbance stability assessment is to determine whether the post-fault system is stable, or whether the point at fault clearance lies inside the region of attraction (ROA) of the post-fault system. In the post-fault system, the OCL is activated and should be considered.

This letter studies large-disturbance stability of the power system with an SG and a CIG connected to infinite bus [2]. Both PLL and OCL are considered. In the timescale of electromechanical transients, the system is simplified to second-order differential-algebraic equation (DAE), and the composition of boundary of ROA is clarified. Different instability patterns in the power system and the corresponding relationship with the characteristics of the boundary of ROA are studied. The effect of OCL on the stability of the power system is discussed to show the necessity of considering OCL in stability analysis.

II. Power System Modelling

The same power system as in [2] is built, which is shown in Fig. 1. The CIG uses grid-following voltage source converter (VSC) for grid integration. In Fig. 1, $E_g\angle\delta_g$ is the internal voltage of the SG; $U_0\angle 0$ is the infinite bus voltage; P_{in} is the power from the DC side of the VSC; C is the DC capacitor of the VSC; and X_{g1}, X_{g2}, and X_{g3} are the line reactances. The following widely adopted assumptions [2], [3] are also adopted.

Manuscript received: February 1, 2023; revised: June 4, 2023; accepted: August 26, 2023. Date of CrossCheck: August 26, 2023. Date of online publication: September 12, 2023.

This work was supported by the National Natural Science Foundation of China (No. U2066602).

L. Chen (corresponding author), Y. Min, L. Hao, and G. Xing are with Department of Electrical Engineering, Tsinghua University, Beijing 100084, China (e-mail: chenlei08@tsinghua.edu.cn; minyong@tsinghua.edu.cn; hls20@mails.tsinghua.edu.cn; xinggz19@mails.tsinghua.edu.cn).

Y. Li and S. Xu are with China Electric Power Research Institute, Beijing 100192, China (e-mail: liyalou@epri.sgcc.com.cn; xushiyun@epri.sgcc.com.cn).

DOI: 10.35833/MPCE.2023.000051

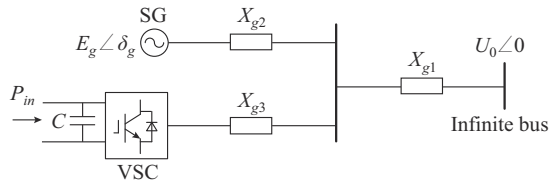

Fig. 1. Diagram of power system where a SG and a VSC are connected to infinite bus.

1) The dynamics of the current control loop (hundreds of hertz) of the VSC are ignored, because they are much faster than the rotor motion dynamics (typically 0.1-2 Hz) of the SG. The q-axis current I_q is 0 in the post-fault system, since the OCL is activated and the control strategy $I_q=0$ is widely used. During grid fault, the OCL is deactivated and the VSC provides reactive power support, i.e., $I_q>0$.

2) The electromagnetic transients of the line are ignored, also because they are much faster than the rotor motion dynamics. Moreover, the effect of frequency on line reactance is ignored because the variation of frequency during a grid fault is small, and the line resistance is 0, since the resistance is much smaller than the reactance in transmission network.

3) The SG adopts the classic model, i.e., a constant internal voltage behind a transient reactance, which is already included in X_{g2}. This model is widely used in the mechanism study of transient stability. A detailed model of SG, the excitation system, and the governor system certainly affect the stability of the power system, but this classic model is still adequate for mechanism study.

The rotor swing equation of the SG is:

$$\begin{cases}\dot{\delta}_g=\omega_0\omega_g\\ T_J\dot{\omega}_g=P_m-P_e-D\omega_g\end{cases}\tag{1}$$

where ω_0 is the rated angular speed; ω_g is the angular speed in p.u.; T_J is the inertia time constant; P_m is the mechanical power; D is the damping coefficient; and P_e is the electromagnetic power expressed by $P_e=\dfrac{E_gU_0\sin\delta_g}{X_{g1}+X_{g2}}-K_1E_g(\cos(\delta_g-\delta_p)I_d+\sin(\delta_g-\delta_p)I_q)$, $K_1=X_{g1}/(X_{g1}+X_{g2})$, δ_p is the phase angle of PLL of the VSC, and I_d is the d-axis current of the VSC.

The equation of the PLL is:

$$\begin{cases}\dot{\delta}_p=k_{p,pll}U_q+k_{i,pll}x_{pll}\\ \dot{x}_{pll}=U_q\end{cases}\tag{2}$$

where x_{pll} is the integral state variable of PLL; $k_{p,pll}$ and $k_{i,pll}$ are the proportional and integral coefficients, respectively; and U_q is the q-axis component of terminal voltage, $U_q=K_1E_g\sin(\delta_g-\delta_p)-K_2U_0\sin\delta_p+X_{g5}I_d$, $K_2=X_{g2}/(X_{g1}+X_{g2})$, $X_{g5}=X_{g3}+X_{g4}$, and $X_{g4}=X_{g1}X_{g2}/(X_{g1}+X_{g2})$.

Since $I_q=0$, only the active power of OCL is considered. The DC voltage control is adopted and the equation is:

$$\begin{cases}CU_{dc}\dot{U}_{dc}=P_{in}-P_c\\ \dot{x}_{dc}=U_{dc}-U_{dcref}\end{cases}\tag{3}$$

where U_{dc} is the DC voltage; U_{dcref} is the corresponding reference value; x_{dc} is the integral state variable of OCL; and $P_c=U_dI_d+U_qI_q$ is the output power of VSC, $I_d=k_{p,dc}(U_{dc}-U_{dcref})+k_{i,dc}x_{dc}$, $U_d=K_1E_g\cos(\delta_g-\delta_p)+K_2U_0\cos\delta_p-X_{g5}I_q$, and $k_{p,dc}$ and $k_{i,dc}$ are the proportional and integral coefficients, respectively.

The following models are then obtained.

A. Model A-D

The OCL is activated, and I_d is the output of the OCL. The dynamics of OCL and PLL are included, and the system model, denoted as model A-D, is composed of (1)-(3).

Since the OCL is activated after fault clearance, model A-D is the actual model of the post-fault system. However, the model with the deactivated OCL, which is widely used in existing studies, is also presented for comparison.

B. Model B-D

The OCL is deactivated, and I_d is constant. Only the dynamics of PLL are included, and the system model, denoted as model B-D, is composed of (1) and (2).

The parameters of PLL and OCL are $k_{p,pll}=30$, $k_{i,pll}=6000$, $C=0.05$, $U_{dcref}=1$, $k_{p,dc}=2$, $k_{i,dc}=4$. Other system parameters can be found in [2] except $D=5.0$.

III. Model Simplification

Obviously, both detailed model A-D and model B-D are multi-timescale. The timescales of the dynamics of PLL shown in (2) and OCL shown in (3), which are often tens of hertz, are much smaller than that of the rotor motion dynamics of SG shown in (1), which is widely known as the timescale of electromechanical transients. For a multi-timescale system, it is well known and widely used that the fast dynamics can be neglected and represented with algebraic equations to reduce the order of the model [4]. Then, the following simplified models, which are DAEs, can be obtained.

A. Model A-S

Neglect the dynamics of both OCL and PLL, and set (2) and (3) to be 0. After careful derivations, we can obtain:

$$g_A(\delta_g,\delta_p)=K_1E_g\sin(\delta_g-\delta_p)-K_2U_0\sin\delta_p+\frac{X_{g5}P_{in}}{K_1E_g\cos(\delta_g-\delta_p)+K_2U_0\cos\delta_p-X_{g5}I_q}=0\tag{4}$$

The simplified model, denoted as model A-S, is DAE and composed of (1) and (4).

B. Model B-S

Neglecting the dynamics of PLL, i.e., (2), implies:

$$g_B(\delta_g,\delta_p)=K_1E_g\sin(\delta_g-\delta_p)-K_2U_0\sin\delta_p+X_{g5}I_d=0\tag{5}$$

The simplified model, denoted as model B-S, is DAE composed of (1) and (5). Model B-S is the model adopted in [2]. The model is only valid when the OCL is deactivated. When the OCL is activated, it is not reasonable to regard I_d as constant in the timescale of electromechanical transients which are much slower than the OCL. Model A-S should be adopted. In the following text, we will show that it is necessary to consider the OCL when studying the large-distur-

bance stability of the power system.

The simplified models, i. e., model A-S and model B-S, are both second-order DAEs, and the validity of the simplification in large-disturbance stability analysis can be verified by the following ROA studies.

IV. Composition of Boundary of ROA

The simplified models A-S and B-S can be represented as:

$$\begin{cases} \dot{\boldsymbol{x}} = \boldsymbol{f}(\boldsymbol{x},\boldsymbol{y}) \\ \boldsymbol{0} = \boldsymbol{g}(\boldsymbol{x},\boldsymbol{y}) \end{cases} \tag{6}$$

where $\boldsymbol{x}=[\delta_g, \omega_g]^{\mathrm{T}}$; $\boldsymbol{y}=\boldsymbol{\delta}_p$; $\dot{\boldsymbol{x}}=\boldsymbol{f}(\boldsymbol{x},\boldsymbol{y})$ is (1); and $\boldsymbol{g}(\cdot)$ is $\boldsymbol{g}_A(\cdot)$ for case A and $\boldsymbol{g}_B(\cdot)$ for case B, respectively.

We study the ROA of simplified models. According to the theorem on boundary of ROA in [5], we should focus on the equilibrium points (EPs) and singular points of the power system.

The EPs are the solutions of (7), which include stable equilibrium points (SEPs) and unstable equilibrium points (UEPs), distinguished by their stabilities.

$$\begin{cases} \boldsymbol{f}(\boldsymbol{x},\boldsymbol{y}) = \boldsymbol{0} \\ \boldsymbol{g}(\boldsymbol{x},\boldsymbol{y}) = \boldsymbol{0} \end{cases} \tag{7}$$

Define $\Delta(\boldsymbol{x},\boldsymbol{y})=\det(D_y\boldsymbol{g}(\boldsymbol{x},\boldsymbol{y}))$, where $\det(\cdot)$ is the determinant of a matrix, $D_y\boldsymbol{g}(\boldsymbol{x},\boldsymbol{y})=\partial\boldsymbol{g}/\partial\boldsymbol{y}\big|_{(\boldsymbol{x},\boldsymbol{y})}$. The singular surface, which is the set of singular points, is defined as:

$$\boldsymbol{S}=\{(\boldsymbol{x},\boldsymbol{y}):\boldsymbol{g}(\boldsymbol{x},\boldsymbol{y})=\boldsymbol{0}, \Delta(\boldsymbol{x},\boldsymbol{y})=\boldsymbol{0}\} \tag{8}$$

At a singular point, $D_y\boldsymbol{g}(\boldsymbol{x},\boldsymbol{y})$ is singular.

Define $\kappa(\boldsymbol{x},\boldsymbol{y})=\mathrm{adj}(D_y\boldsymbol{g}(\boldsymbol{x},\boldsymbol{y}))D_x\boldsymbol{g}(\boldsymbol{x},\boldsymbol{y})\boldsymbol{f}(\boldsymbol{x},\boldsymbol{y})$, where $\mathrm{adj}(\cdot)$ is the adjoint matrix of a matrix. The semi-singular surface, which is the set of semi-singular points (SSPs), is defined as:

$$\boldsymbol{\Xi}=\{(\boldsymbol{x},\boldsymbol{y})\in\boldsymbol{S}:\kappa(\boldsymbol{x},\boldsymbol{y})\neq\boldsymbol{0}, D_y\Delta(\boldsymbol{x},\boldsymbol{y})\kappa(\boldsymbol{x},\boldsymbol{y})=\boldsymbol{0}\} \tag{9}$$

The trajectory through an SSP is tangential to the singular surface.

For model A-S, the singular points are the solutions of:

$$\begin{cases} \boldsymbol{g}_A = \boldsymbol{0} \\ \partial\boldsymbol{g}_A/\partial\boldsymbol{\delta}_p = \boldsymbol{0} \end{cases} \tag{10}$$

Denote the solution as $(\delta_{g,spA}, \delta_{p,spA})$ and ω_g is arbitrary. In the plane of (δ_g, ω_g), the singular surface is the vertical line $\delta_g=\delta_{g,spA}$. Obviously, when $\omega_g=0$, the vector $\boldsymbol{f}(\boldsymbol{x},\boldsymbol{y})$ is tangential to the line, which means the trajectory is tangential to the singular surface. Therefore, the SSP is $(\delta_{g,spA}, 0)$.

For model B-S, the singular points are the solutions of

$$\begin{cases} \boldsymbol{g}_B = \boldsymbol{0} \\ \partial\boldsymbol{g}_B/\partial\boldsymbol{\delta}_p = \boldsymbol{0} \end{cases} \tag{11}$$

Denote the solution as $(\delta_{g,spB}, \delta_{p,spB})$. With the same analysis, we can get that the singular surface is the vertical line $\delta_g=\delta_{g,spB}$, and the SSP is $(\delta_{g,spB}, 0)$.

According to the theorem in [5], the boundary of ROA of model A-S (and model B-S) is composed of: ① stable manifolds of UEPs on the boundary; ② stable manifolds of SSPs on the boundary; and ③ singular surface pieces.

Consider the three cases with different outputs of SG and CIG, as shown in Table I. The SEPs of models A and B are identical. The compositions of boundary of ROA are shown in Fig. 2 and Table I. The stable manifolds of UEP or SSP are plotted with thick solid lines, and the singular surface pieces are plotted with thick dashed lines. Blue lines are for model A and red lines are for model B. UEP_A and UEP_B are the UEPs of models A and B, respectively.

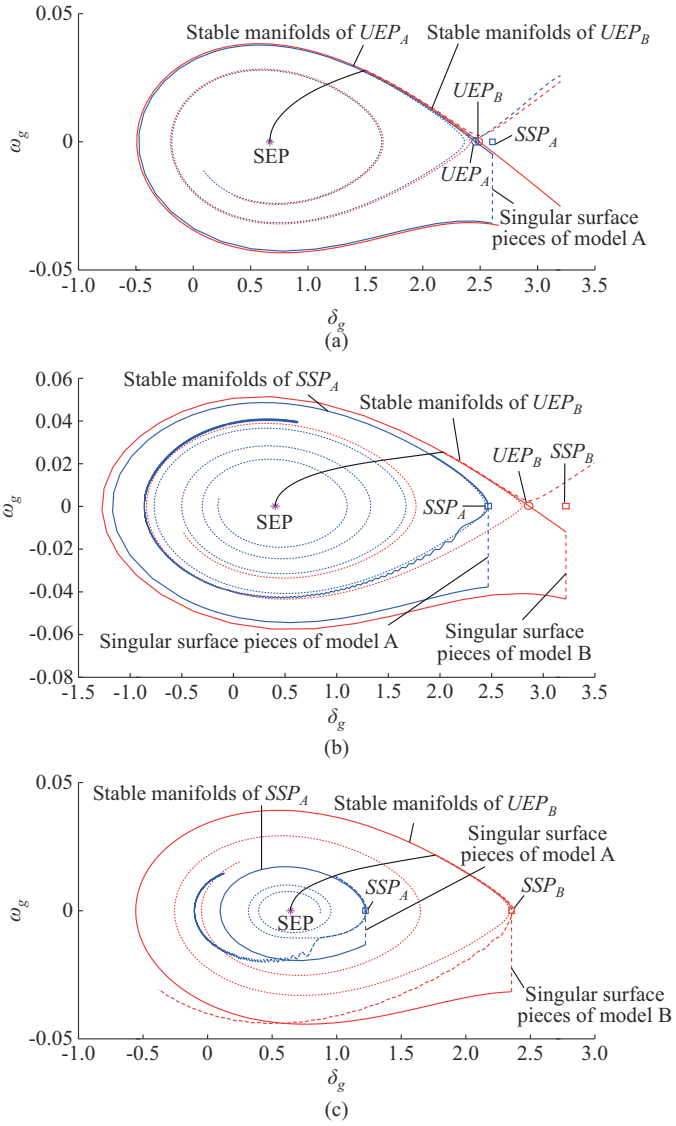

Fig. 2. Boundary of ROA of simplified model as well as fault-on, critically stable, and critically unstable trajectories of detailed model. (a) Case 1. (b) Case 2. (c) Case 3.

TABLE I
Composition of Boundary of ROA

Case	Parameters	Composition of boundary of ROA	
		Model A-S	Model B-S
Case 1	$P_m=1.5$, $I_d=0.1$, $P_{in}=0.1006$	Stable manifolds of UEP and singular surface pieces	Stable manifolds of UEP
Case 2	$P_m=1.0$, $I_d=0.2$, $P_{in}=0.2069$	Stable manifolds of SSP and singular surface pieces	Stable manifolds of UEP and singular surface pieces
Case 3	$P_m=1.0$, $I_d=1.0$, $P_{in}=0.9227$	Stable manifolds of SSP and singular surface pieces	Stable manifolds of SSP and singular surface pieces

Time-domain simulations in the detailed models, i.e., model A-D and model B-D, are also carried out. The fault is the drop of the infinite bus voltage to 0.3 p.u.. During the fault, the CIG switches to current-controlled mode with $I_d=0$ and I_q=1.0. After the fault, the OCL is activated again. Increase the duration time of the fault to get the critically stable and critically unstable cases. The trajectories are also plotted in Fig. 2. The black thin lines, dotted thin lines (blue/red for model A-D/B-D), and dashed thin lines (blue/red for model A-D/B-D) are fault-on, critically stable, and critically unstable trajectories, respectively. It can be observed that separation point of the critically stable trajectory and the critically unstable trajectory is very close to the boundary of ROA computed with the simplified model, which verifies the validity of the simplified model as well as the boundary of ROA.

V. Anchor Point and Dominant Instability Pattern

Both UEPs and SSPs on the boundary of ROA are named anchor points in [5]. The type of anchor point actually determines the dominant instability pattern of the power system.

When the anchor point is UEP and the boundary of ROA is composed of stable manifolds of UEP, the dominant instability pattern of the system is conventional rotor angle instability of SG, in which the rotor angle of SG diverges. Case 1 is this situation, whether the OCL is activated or deactivated. The divergence of δ_g with the unstable trajectories (dashed thin lines) can be clearly observed in Fig. 2(a). This form of instability is typical in traditional power systems, and will not be discussed in detail here.

When the anchor point is SSP and the boundary of ROA is composed of stable manifolds of SSP, the dominant instability pattern of the system is instability of PLL and OCL of VSC. Case 3 is this situation, whether the OCL is activated or not. The critically stable and critically unstable trajectories of detailed models in Fig. 2(c) are plotted in time domain and shown in Fig. 3. How to get the trajectories is described in Section IV. We first study model A-D with the OCL activated, which is the actual model of the post-fault system. The results are shown in Fig. 3(a). We examine the inputs of the PI segments of PLL and OCL, i. e., U_q and ΔU_{dc}, respectively. The control targets of PLL and OCL are $U_q=0$ and $\Delta U_{dc}=0$, respectively. We can observe U_q or ΔU_{dc} to see whether PLL or OCL achieves its target. When PLL or OCL achieves its target, it can be deemed stable, and vice versa. In Fig. 3(a), we can clearly see that U_q and ΔU_{dc} diverge just after δ_g encounters the singular points $\delta_{g,spA}$, while δ_g does not diverge and still remains at reasonable values. The instability pattern is the instability of PLL and OCL of VSC.

The results of model B-D with OCL deactivated, although not actual, are also presented in Fig. 3(b). Similar phenomena can be observed. U_q diverges just after δ_g encounters the singular points $\delta_{g,spB}$, which means the instability pattern is the instability of PLL of VSC, since the OCL is deactivated in this model.

From the results, the relation between the simplified model and the detailed model can be illustrated. Singularity of algebraic equations in the simplified model corresponds to instability of fast dynamics in the detailed model, which are neglected and represented with algebraic equations in the simplified model.

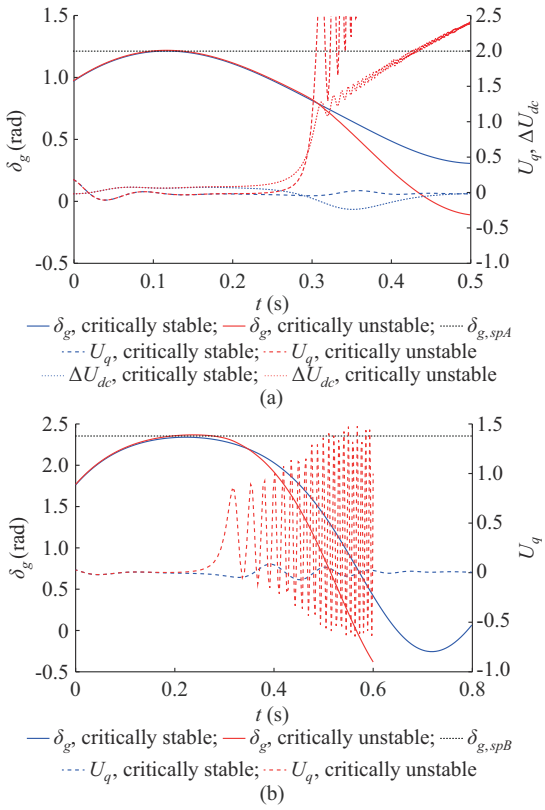

Fig. 3. Critically stable and critically unstable trajectories in time domain. (a) Model A. (b) Model B.

Therefore, we can examine the type of anchor point to determine the dominant instability pattern of the system. In the UEP and the SSP of the system, $\omega_g=0$ and δ_g are different. δ_g of the UEP, denoted as $\delta_{g,uep}$, is the solution of (7), and δ_g of the SSP, denoted as $\delta_{g,spA}$, is the solution of (10). The smaller one is the anchor point. We can compare the values of $\delta_{g,uep}$ and $\delta_{g,spA}$ to determine the dominant instability pattern of the system. When $\delta_{g,uep}<\delta_{g,spA}$, the anchor point is UEP, and the dominant instability pattern is rotor angle instability of SG. When $\delta_{g,uep}>\delta_{g,spA}$, the anchor point is SSP, and the dominant instability pattern is instability of PLL and OCL of VSC. When $\delta_{g,uep}=\delta_{g,spA}$, it is the critical situation.

With the proposed criteria, we can analyze the effect of active power of SG and VSC on the instability pattern of the system with the OCL activated, as shown in Fig. 4. As P_m decreases or P_{in} increases, the dominant instability pattern of the system changes from rotor angle instability of SG to instability of PLL and OCL of VSC, and vice versa. This is rational and consistent with common understanding. The line in Fig. 4 represents the critical situations or the transition points of dominant instability pattern. Transition of dominant instability pattern can be quantitatively analyzed. When the OCL is deactivated, the vertical axis of Fig. 4 should be changed to I_d, although this is not reasonable because the

OCL is activated and should be considered in post-fault system.

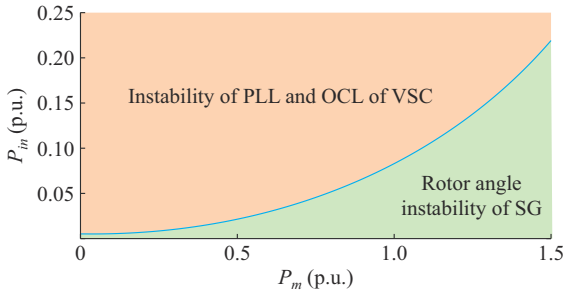

Fig. 4. Change of dominant instability pattern with active power of SG and VSC.

It should be noted that dominant instability pattern only means the instability can be observed more obviously on the variables of the SG or VSC, but does not mean their interplay can be ignored. From Fig. 3, it can be clearly observed that the instability of VSC is induced by the motion of the rotor angle of SG, and from Fig. 2(b), it can be observed that the control strategy of VSC (OCL activated or deactivated) affects the stability of the SG. However, this letter focuses on instability pattern affected by the interplay between SG and VSC; how the interplay affects the degree of stability of the system still needs further investigation.

Time domain simulations are also carried out in the system with full models of SG and VSC. The SG adopts the 6$^{\text{th}}$-order generator model and is equipped with AVR and PSS. The VSC adopts the model containing PLL, DC voltage control loop, and current control loop. The results are shown in Fig. 5. As described above, the dominant instability pattern of Case 1 is rotor angle instability of SG. Figure 5(a) clearly shows the divergence of δ_g, which further induces instability of PLL and OCL of VSC, corresponding to the encounter with singular points in Fig. 2(a). The dominant instability pattern of Case 3 is instability of PLL and OCL of VSC. In Fig. 5(b), δ_g does not diverge, but U_q and ΔU_{dc} diverge, which means PLL and OCL of VSC lose stability. The results of the full model are consistent with previous analyses in this letter.

VI. Effect of Outer Control Loop

As shown in Fig. 2, in all the cases, the ROA of model B with the OCL activated lies in and is smaller than the ROA of model A with the OCL deactivated, especially when the active power of VSC is large. Therefore, the OCL worsens large disturbance of the system. Furthermore, from Fig. 2(b), it can be observed that when the OCL is activated, the system is more prone to VSC instability, in which the boundary of ROA is composed of stable manifolds of SSP. The OCL has great effect on both the degree and the pattern of the stability of the system, and should be considered seriously.

During a fault, the OCL is re-activated after the VSC quits the low-voltage ride-through mode. The way of not considering the OCL is only valid for the fault-on system. It is necessary to consider the OCL when studying the large-disturbance stability of the power system.

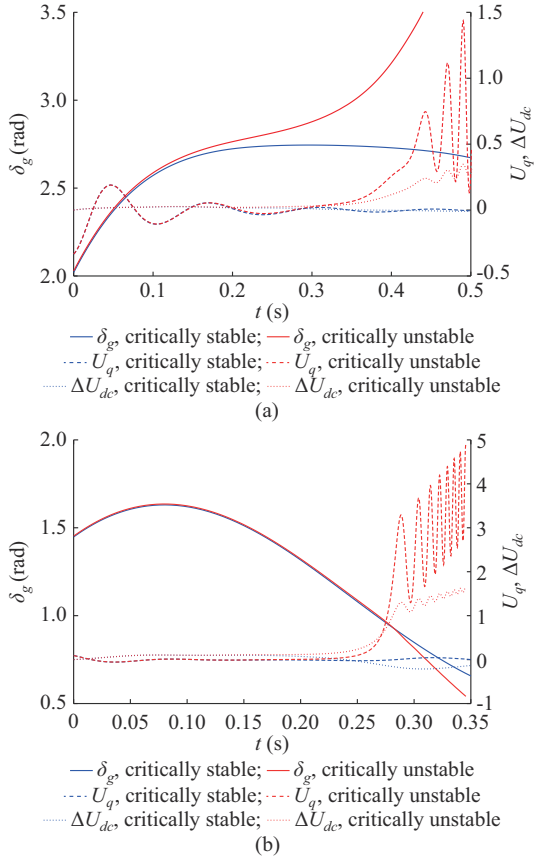

Fig. 5. Simulation results of power system with full models. (a) Case 1. (b) Case 3.

VII. Conclusion

Large-disturbance stability of power system with a SG and a CIG connected to infinite bus is studied. Simplified models, which are second-order DAEs, are built for both situations, where the OCL is deactivated and activated. The findings are as follows. The boundary of the simplified model is composed of stable manifolds of UEP or SSP, named anchor points and singular surface pieces. When the anchor point is UEP, the dominant instability pattern of the system is rotor angle instability of SG. When the anchor point is SSP, the dominant instability pattern of the system is instability of PLL and OCL of VSC. Relative position relationship between UEP and SSP can be used to quantitatively analyze the transition of dominant instability pattern of the system. The OCL has significant effect on the large-disturbance stability of the system. When the OCL is activated, the ROA becomes smaller and the system is more prone to VSC instability, which shows the necessity of considering OCL. The findings of this letter are helpful for the insight into the large-disturbance stability of power systems with both SGs and CIGs. Future work will focus on the stability of power system with multiples SGs and CIGs.

References

[1] H. N. V. Pico and B. B. Johnson, "Transient stability assessment of multi-machine multi-converter power systems," *IEEE Transactions on Power Systems*, vol. 34, no. 5, pp. 3504-3514, Sept. 2019.

[2] X. He and H. Geng, "Transient stability of power systems integrated

with inverter-based generation," *IEEE Transactions on Power Systems*, vol. 36, no. 1, pp. 553-556, Jan. 2021.
[3] Y. Gu and T. C. Green, "Power system stability with a high penetration of inverter-based resources," *Proceedings of the IEEE*, vol. 111, no. 7, pp. 832-853, Jul. 2023.
[4] E. C. Pillco and L. F. C. Alberto, "On the foundations of stability analysis of power systems in time scales," *IEEE Transactions on Circuits and Systems – I: Regular Papers*, vol. 62, no. 5, pp. 1230-1239, May 2015.
[5] V. Venkatasubramanian, H. Schattler, and J. Zaborszky, "Dynamics of large constrained nonlinear systems – a taxonomy theory," *Proceedings of the IEEE*, vol. 83, no. 11, pp. 1530-1561, Nov. 1995.

Lei Chen received the B. Sc. and Ph. D. degrees in electrical engineering from Tsinghua University, Beijing, China, in 2003 and 2008, respectively. Since 2008, he has been with the Department of Electrical Engineering, Tsinghua University, where he is currently an Associate Professor. He was a Recipient of the Excellent Young Scientists Fund of the National Natural Science Foundation of China in 2019. His research interests include dynamic analysis and control of power systems.

Yong Min received the B. S. and Ph. D. degrees in electrical engineering from the Department of Electrical Engineering, Tsinghua University, Beijing, China, in 1984 and 1990, respectively. He is currently a Professor in the Department of Electrical Engineering, Tsinghua University. He is a Fellow of the Institution of Engineering and Technology. His research interests include power system dynamic analysis and smart grid technology.

Liangshuai Hao received the B.S. degree in electrical engineering and automation from the School of Electrical Engineering at Shandong University, Jinan, China, in 2020. He is currently working towards the M. S. degree in electrical engineering at Tsinghua University, Beijing, China. His current research interests mainly include stability and control of power system with high proportion of power electronic devices.

Guangzheng Xing received the B. S. and M. S. degrees in electrical engineering from Tsinghua University, Beijing, China, in 2017 and 2019, respectively, where he has been working toward the Ph.D. degree in electrical engineering since 2019. His research interests include stability of power system with high penetration of renewables and inverters.

Yalou Li received the bachelor's degree in electrical engineering from Huazhong University of Science and Technology, Wuhan, China, in 1997, and the master's and Ph. D. degrees in electrical engineering from the China Electric Power Research Institute, Beijing, China, in 2000 and 2003, respectively. He is currently a Chief Engineer with the Power System Department, China Electric Power Research Institute. His current research interests include digital simulation, analysis, and control of AC and DC power systems and key devices.

Shiyun Xu received the Ph. D. degree in mechanical systems and control from Peking University, Beijing, China, in 2010, under the direction of Prof. Lin Huang. Then, she worked as a Postdoctoral Fellow with the China Electric Power Research Institute, Beijing, China, till 2012. From 2007 to 2008, she was a Visiting Scholar at Polytechnic Institute, New York University, New York, USA, hosted by Prof. Zhongping Jiang. Currently, she is a Professor-level Senior Engineer at China Electric Power Research Institute. Her research interests include dynamic stability analysis and control of power systems with high penetration of renewable energies.